Supplement of

Mixing state and effective density of aerosol particles during the Beijing 2022 Olympic Winter Games

Aodong Du[1,2], Jiaxing Sun[1,2], Hang Liu[1], Weiqi Xu[1], Wei Zhou[1], Yuting Zhang[1,2], Lei Li[3], Xubing Du[3,4], Yan Li[1,2], Xiaole Pan[1], Zifa Wang[1,2], and Yele Sun[1,2]

[1]State Key Laboratory of Atmospheric Boundary Layer Physics and Atmospheric Chemistry, Institute of Atmospheric Physics, Chinese Academy of Sciences, Beijing 100029, China

[2]College of Earth and Planetary Sciences, University of Chinese Academy of Sciences, Beijing 100049, China

[4]Institute of Mass Spectrometry and Atmospheric Environment, Jinan University, Guangzhou 510632, China

[5]Guangdong Provincial Engineering Research Center for On-Line Source Apportionment System of Air Pollution, Guangzhou 510632, China

Correspondence to: Yele Sun (sunyele@mail.iap.ac.cn)

Table S1: Summary of the sampling periods, the number of hit particles, the average mass concentrations of NR-PM_1 and eBC, and the average absorption Ångström exponent (AAE) for different particle size-selection periods.

	Duration	MASS	NR-PM_1 (μg m^{-3})	eBC (μg m^{-3})	AAE
D_m=200nm	1.21-2.2	320093	23.93	2.12	1.40
D_m=250nm	2.2-2.5	37498	2.46	0.36	1.49
D_m=300nm	2.5-2.8	32909	2.85	0.46	1.48
D_m=150nm	2.8-2.10	46651	10.69	1.80	1.48
D_a=300nm	2.11-3.1	322415	8.70	1.16	1.37

Table S2: Description of the different particle classes and summary of the characteristic peaks.

Description of different classes	Characteristic peaks
pure-EC	$C_n^{\pm}$, n = 1, 2, 3… (Xie et al., 2020; Liu et al., 2019)
EC internally mixed with nitrate and sulfate (EC-NS)	46$[NO_2]^-$, 62$[NO_3]^-$ and $C_n^{\pm}$ (Chen et al., 2020; Dall'osto and Harrison, 2012)
K rich EC, internally mixed with nitrate (KEC-N)	39$[K]^+$, 46$[NO_2]^-$, 62$[NO_3]^-$ and $C_n^{\pm}$ (Li et al., 2014; Healy et al., 2013)
K and Na rich EC, internally mixed with nitrate (KNaEC-N)	39$[K]^+$, 23$[Na]^+$, 46$[NO_2]^-$, 62$[NO_3]^-$ and $C_n^{\pm}$ (Li et al., 2018; Toner et al., 2008)
ECOC internally mixed with nitrate and sulfate (ECOC-NS)	46$[NO_2]^-$, 62$[NO_3]^-$, 97$[HSO_4]^-$, $C_n^{\pm}$ and OC peaks (including 27$[C_2H_3]^+$, 37$[C_3H]^+$, 43$[C_2H_3O]^+$, 50$[C_4H_2]^+$, 51$[C_4H_3]^+$…) (Sun et al., 2022a; Sun et al., 2022b; Xie et al., 2020)
K rich ECOC, internally mixed with nitrate and sulfate (KECOC-NS)	39$[K]^+$, 46$[NO_2]^-$, 62$[NO_3]^-$, 97$[HSO_4]^-$, $C_n^{\pm}$ and OC peaks (Moffet et al., 2008; Zhang et al., 2008)
K rich ECOC, internally mixed with cyanide (KECOC-CN)	39$[K]^+$, 26$[CN]^-$, 42$[CNO]^-$, $C_n^{\pm}$ and OC peaks (Lu et al., 2017; Pratt et al., 2009)
K and Na rich ECOC, internally mixed with nitrate and sulfate (KNaECOC-NS)	39$[K]^+$, 23$[Na]^+$, 46$[NO_2]^-$, 62$[NO_3]^-$, 97$[HSO_4]^-$, $C_n^{\pm}$ and OC peaks (Li et al., 2014; Gard et al., 1998)

K rich ECOC, internally mixed with nitrate, sulfate and ammonium (KAECOC-NS)	39$[K]^+$, 18$[NH_4]^+$, 46$[NO_2]^-$, 62$[NO_3]^-$, 97$[HSO_4]^-$, $C_n^{\pm}$ and OC peaks (Zhong et al., 2022; Gross et al., 2000)
K rich OC, internally mixed with nitrate (KOC-N)	39$[K]^+$, 46$[NO_2]^-$, 62$[NO_3]^-$ and OC peaks (Bi et al., 2011)
K rich OC, internally mixed with nitrate and sulfate (KOC-NS)	39$[K]^+$, 46$[NO_2]^-$, 62$[NO_3]^-$, 97$[HSO_4]^-$ and OC peaks (Spencer et al., 2007; Bi et al., 2011)
K rich organic amine, internally mixed with nitrate and sulfate (K-Amine-NS)	39$[K]^+$, 58$[C_3H_8N]^+$, 59$[C_3H_9N]^+$, 46$[NO_2]^-$, 62$[NO_3]^-$, 97$[HSO_4]^-$ and OC peaks (Chen et al., 2019; Angelino et al., 2001; Cheng et al., 2018)
K rich particles from biomass combustion (Biomass-K)	39$[K]^+$, 45$[CHO_2]^-$, 59$[C_2H_3O_2]^-$, 71$[C_3H_3O]^-$ and 73$[C_3H_5O_2]^-$ (Hatch et al., 2014; Silva et al., 1999; Guazzotti et al., 2003)
High-molecular-weight organic matter (HOM)	152$[C_{12}H_8]^+$, 165$[C_{13}H_9]^+$, 178$[C_{14}H_{10}]^+$, 189$[C_{15}H_9]^+$… (Zhang et al., 2022; Drewnick et al., 2008; Toner et al., 2006)
K rich particles, internally mixed with nitrate (K-N)	39$[K]^+$, 46$[NO_2]^-$ and 62$[NO_3]^-$ (Dall'osto et al., 2008)
K and Na rich particles, internally mixed with nitrate (KNa-N)	39$[K]^+$, 23$[Na]^+$, 46$[NO_2]^-$ and 62$[NO_3]^-$ (Guo et al., 2010)
Fe rich particles (rich-Fe)	56$[Fe]^+$ and 54$[Fe]^+$ (Wang et al., 2016; Zhang et al., 2014; Furutani et al., 2011)

Table S3: Correlation analysis between the number concentration of each particle type and the mass concentration of the chemical components measured by HR-ToF-AMS. Higher similarities are marked with *.

	FFBBOA	COA	OOA1	OOA2	aqOOA	Org	SO_4	NO_3	NH_4	Chl
pure-EC	0.25	0.47	0.20	-0.03	0.04	0.23	0.01	0.14	0.11	0.24
EC-NS	0.15	0.17	0.75*	0.81*	0.71*	0.76	0.74	0.82	0.82	0.56
KEC-N	0.32	0.27	0.85*	0.79*	0.77*	0.85	0.80	0.87	0.88	0.80*
KNaEC-N	0.74*	0.56	0.69	0.25	0.41	0.67	0.35	0.54	0.50	0.74*

ECOC-NS	0.44	0.14	0.29	0.14	0.27	0.32	0.36	0.25	0.29	0.36
KECOC-NS	0.78*	0.60	0.63	0.31	0.48	0.69	0.45	0.52	0.51	0.67
KECOC-CN	0.27	0.14	-0.09	-0.08	0.13	0.05	0.08	-0.04	0	0.18
KNaECOC-NS	0.80*	0.55	0.70*	0.23	0.41	0.67	0.40	0.51	0.49	0.70*
KAECOC-NS	0.27	0.17	0.77*	0.76*	0.79*	0.79	0.85	0.80	0.84	0.67
KOC-N	0.70*	0.67	0.33	0.06	0.22	0.45	0.12	0.24	0.21	0.45
KOC-NS	0.69	0.72*	0.66	0.31	0.49	0.73	0.47	0.55	0.54	0.71*
K-Amine-NS	0.01	0.03	0.55	0.83*	0.66	0.63	0.69	0.71	0.73	0.45
Biomass-K	0.55	0.73*	0.26	0.12	0.03	0.32	-0.04	0.09	0.06	0.32
HOM	0.47	0.03	-0.07	-0.09	0.11	0.05	0.08	-0.04	-0.01	0.19
K-N	0.62	0.51	0.82*	0.61	0.74*	0.89	0.75	0.79	0.81	0.86*
KNa-N	0.63	0.52	0.54	0.22	0.40	0.58	0.32	0.42	0.40	0.58

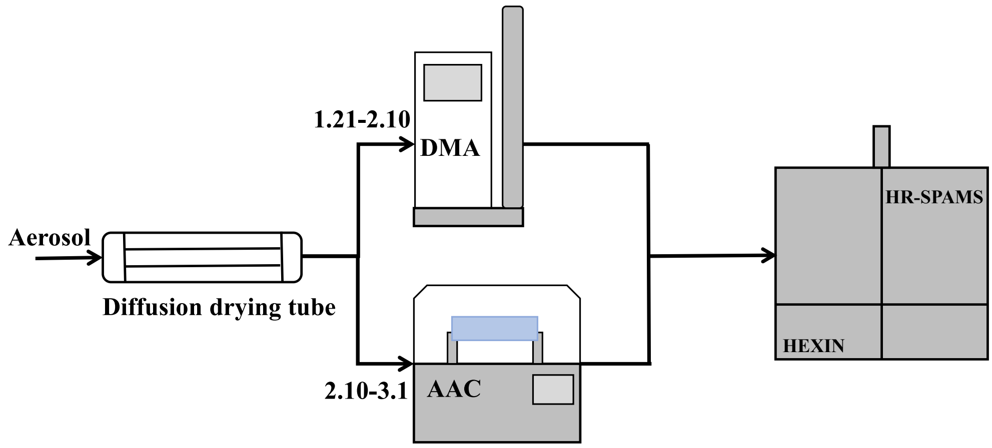

Figure S1: Schematic diagram of the experimental system.

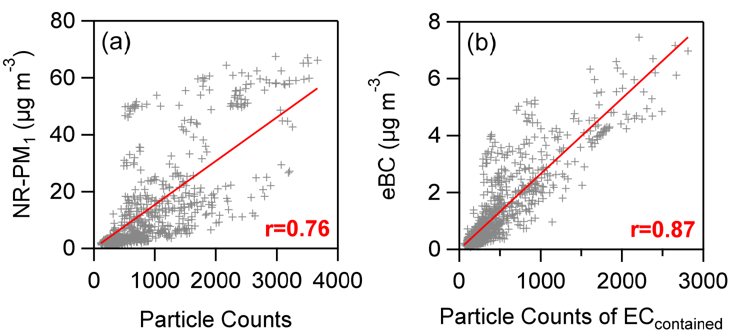

Figure S2: Scatter plots of the (a) total particle counts and (b) EC-containing particle counts captured by SPAMS versus the mass concentration of NR-PM$_1$ and eBC measured by AMS and AE33.

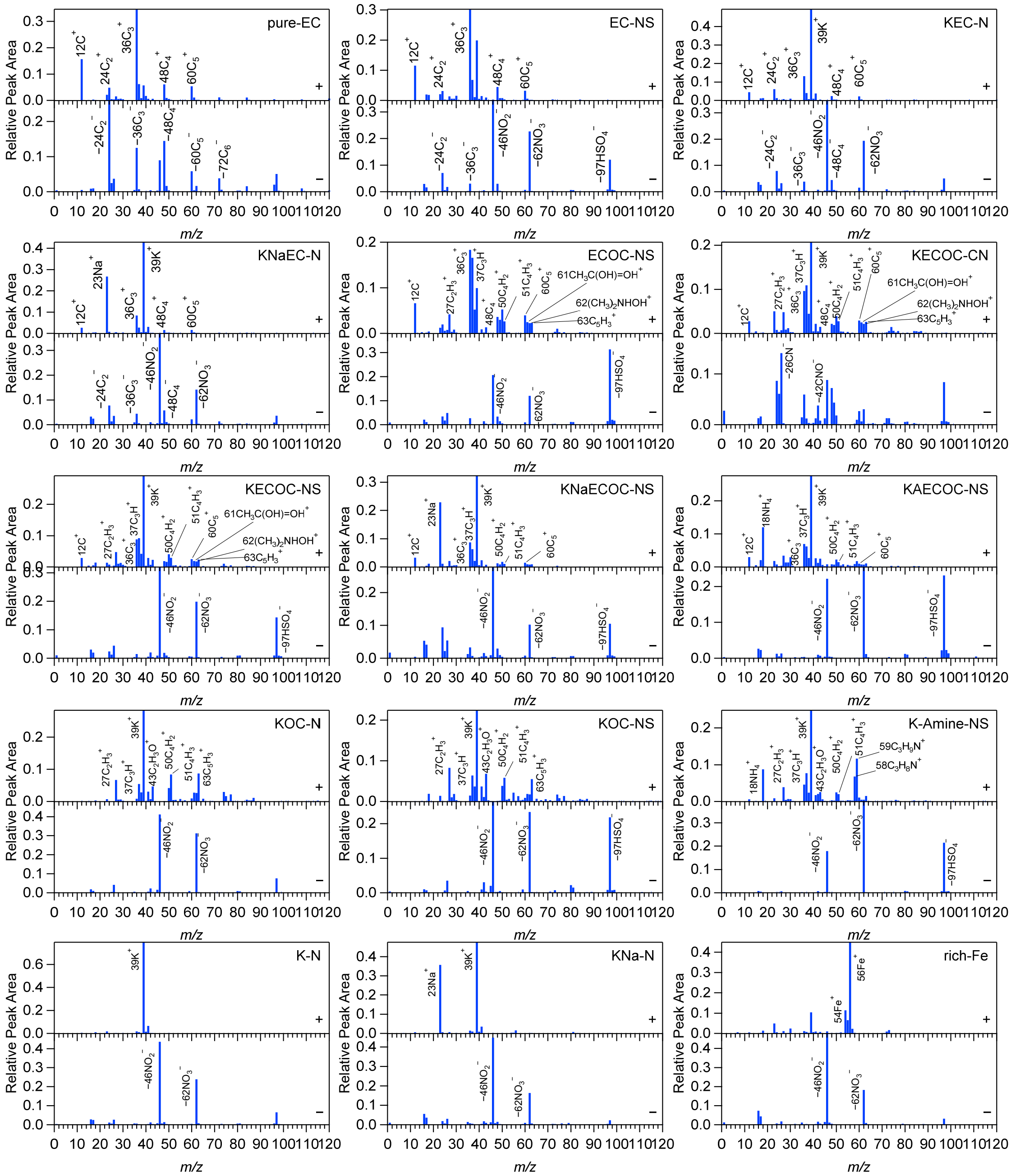

Figure S3: Average mass spectra of each subclass of particles.

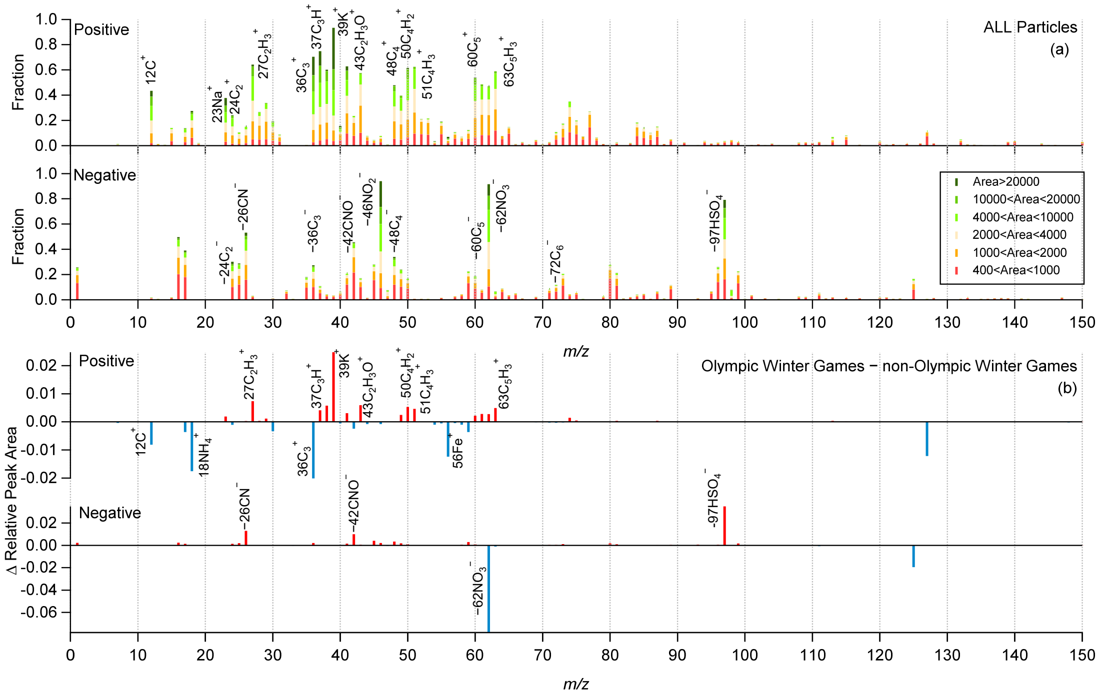

Figure S4: The (a) digital mass spectra of all particles throughout the campaign (where the ion heights in the spectrum represent their proportions and the colors represent the range of peak area intensities), and (b) the differences in the average mass spectra of particles during the Olympic Winter Games and non- Olympic Winter Games periods.

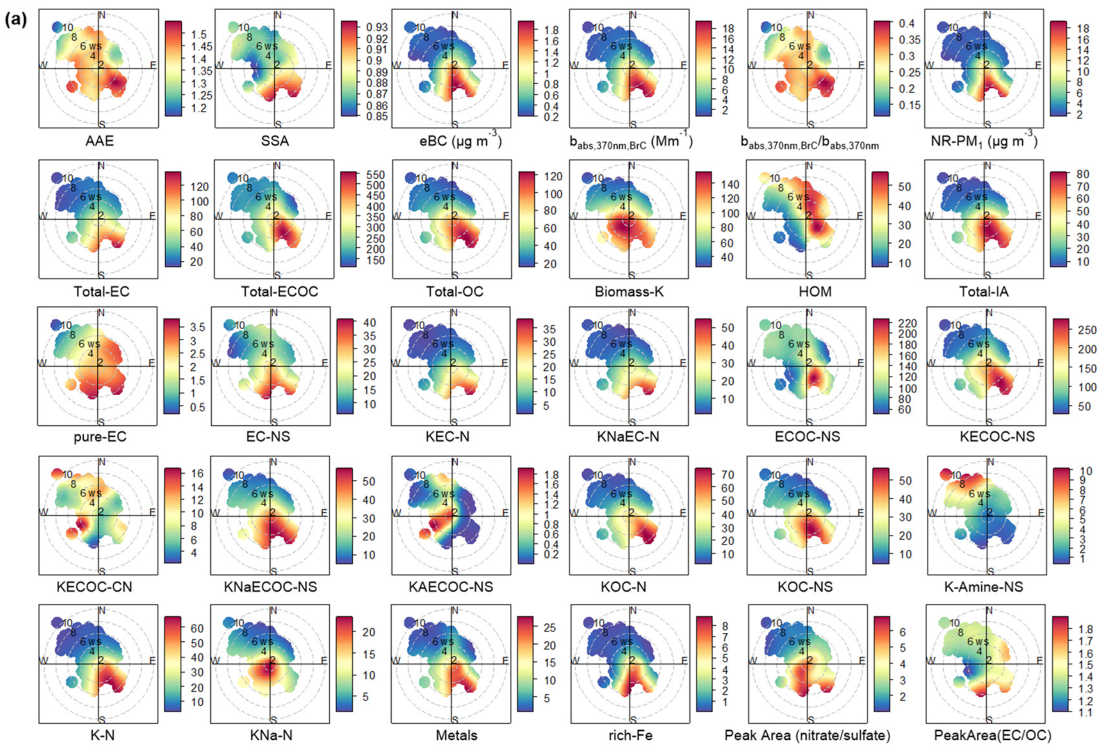

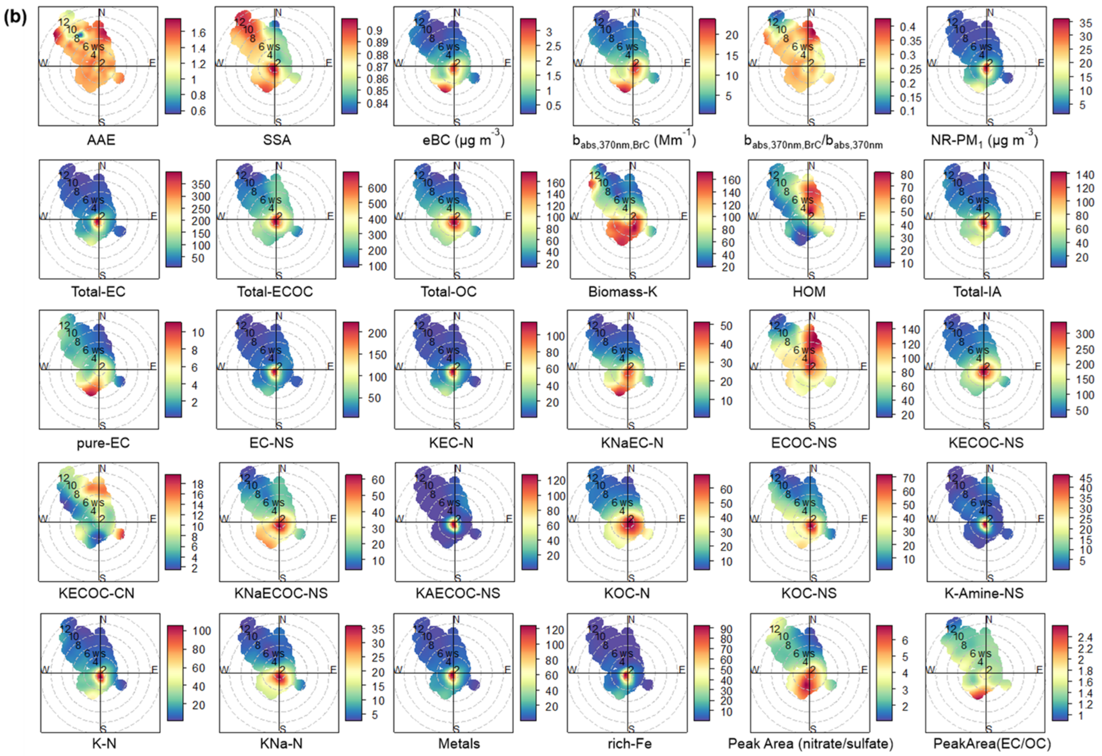

Figure S5: Bivariate polar plots of different types of particles and other parameters during (a) Olympic Winter Games and (b) non-Olympic Winter Games.

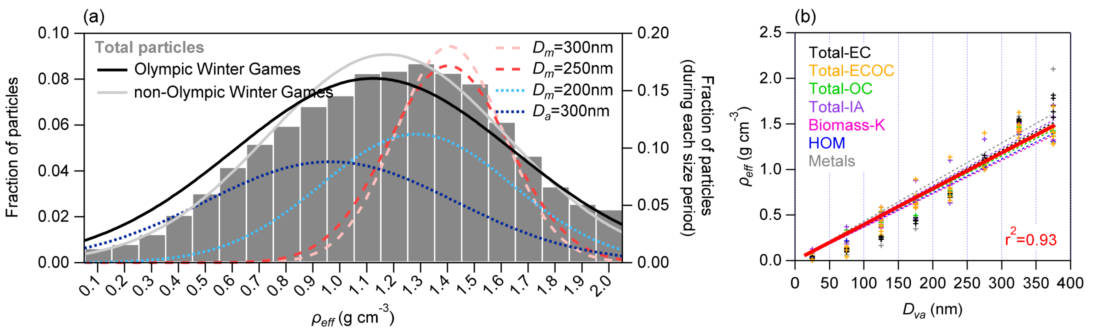

Figure S6: Distributions of effective density of particles for different periods (a). The left y–axis is applied to the column diagram as well as OWG and now periods, and the right y–axis is applied to the Gaussian fitting curves for each size-resolution period. And variations of effective density as a function of D_{va} (b).

References

Angelino, S., Suess, D. T., and Prather, K. A.: Formation of Aerosol Particles from Reactions of Secondary and Tertiary Alkylamines: Characterization by Aerosol Time-of-Flight Mass Spectrometry, Environ. Sci. Technol., 35, 3130-3138, doi:10.1021/es0015444 2001.

Bi, X., Zhang, G., Li, L., Wang, X., Li, M., Sheng, G., Fu, J., and Zhou, Z.: Mixing state of biomass burning particles by single particle aerosol mass spectrometer in the urban area of PRD, China, Atmos. Environ., 45, 3447-3453, doi:10.1016/j.atmosenv.2011.03.034, 2011.

Chen, Y., Tian, M., Huang, R.-J., Shi, G., Wang, H., Peng, C., Cao, J., Wang, Q., Zhang, S., Guo, D., Zhang, L., and Yang, F.: Characterization of urban amine-containing particles in southwestern China: seasonal variation, source, and processing, Atmos. Chem. Phys., 19, 3245-3255, doi:10.5194/acp-19-3245-2019, 2019.

Chen, Y., Cai, J., Wang, Z., Peng, C., Yao, X., Tian, M., Han, Y., Shi, G., Shi, Z., Liu, Y., Yang, X., Zheng, M., Zhu, T., He, K., Zhang, Q., and Yang, F.: Simultaneous measurements of urban and rural particles in Beijing – Part 1: Chemical composition and mixing state, Atmos. Chem. Phys., 20, 9231-9247, doi:10.5194/acp-20-9231-2020, 2020.

Cheng, C., Huang, Z., Chan, C. K., Chu, Y., Li, M., Zhang, T., Ou, Y., Chen, D., Cheng, P., Li, L., Gao, W., Huang, Z., Huang, B., Fu, Z., and Zhou, Z.: Characteristics and mixing state of amine-containing particles at a rural site in the Pearl River Delta, China, Atmos. Chem. Phys., 18, 9147-9159, doi:10.5194/acp-18-9147-2018, 2018.

Dall'Osto, M. and Harrison, R. M.: Urban organic aerosols measured by single particle mass spectrometry in the megacity of London, Atmos. Chem. Phys., 12, 4127-4142, doi:10.5194/acp-12-4127-2012, 2012.

Dall'Osto, M., Booth, M. J., Smith, W., Fisher, R., and Harrison, R. M.: A Study of the Size Distributions and the Chemical Characterization of Airborne Particles in the Vicinity of a Large Integrated Steelworks, Aerosol Sci. Tech., 42, 981-991, doi:10.1080/02786820802339587, 2008.

Drewnick, F., Dall'Osto, M., and Harrison, R.: Characterization of aerosol particles from grass mowing by joint deployment of ToF-AMS and ATOFMS instruments, Atmos. Environ., 42, 3006-3017, doi:10.1016/j.atmosenv.2007.12.047, 2008.

Furutani, H., Jung, J., Miura, K., Takami, A., Kato, S., Kajii, Y., and Uematsu, M.: Single-particle chemical characterization and source apportionment of iron-containing atmospheric aerosols in Asian outflow, J. Geophys. Res., 116, D18204, doi:10.1029/2011jd015867, 2011.

Gard, E. E., Kleeman, M. J., Gross, D. S., Hughes, L. S., Allen, J. O., Morrical, B. D., Fergenson, D. P., Dienes, T., Galli, M. E., Johnson, R. J., Cass, G. R., and Prather, K. A.: Direct observation of heterogeneous chemistry in the atmosphere, Science, 279, 1184-1187, doi:10.1126/science.279.5354.1184, 1998.

Gross, D. S., Galli, M. E., Silva, P. J., and Prather, K. A.: Relative sensitivity factors for alkali metal and ammonium cations in single-particle aerosol time-of-flight mass spectra, Anal Chem, 72, 416-422, doi:10.1021/ac990434g, 2000.

Guazzotti, S. A., Suess, D. T., Coffee, K. R., Quinn, P. K., Bates, T. S., Wisthaler, A., Hansel, A., Ball, W. P., Dickerson, R. R., Neususs, C., Crutzen, P. J., and Prather, K. A.: Characterization of carbonaceous aerosols outflow from India and Arabia: Biomass/biofuel burning and fossil fuel combustion, J. Geophys. Res., 108, 4485, doi:10.1029/2002jd003277, 2003.

Guo, S., Hu, M., Wang, Z., Slanina, J., and Zhao, Y.: Size-resolved aerosol water-soluble ionic compositions in the summer of Beijing: implication of regional secondary formation, Atmos. Chem. Phys., 10, 947–959, doi:10.5194/acp-10-947-2010, 2010, 2010.

Hatch, L. E., Pratt, K. A., Huffman, J. A., Jimenez, J. L., and Prather, K. A.: Impacts of Aerosol Aging on Laser Desorption/Ionization in Single-Particle Mass Spectrometers, Aerosol Sci. Tech., 48, 1050-1058, doi:10.1080/02786826.2014.955907, 2014.

Healy, R. M., Sciare, J., Poulain, L., Crippa, M., Wiedensohler, A., Prévôt, A. S. H., Baltensperger, U., Sarda-Estève, R., McGuire, M. L., Jeong, C. H., McGillicuddy, E., O'Connor, I. P., Sodeau, J. R., Evans, G. J., and Wenger, J. C.: Quantitative determination of carbonaceous particle mixing state in Paris using single-particle mass spectrometer and aerosol mass spectrometer measurements, Atmos. Chem. Phys., 13, 9479-9496, doi:10.5194/acp-13-9479-2013, 2013.

Li, K., Ye, X., Pang, H., Lu, X., Chen, H., Wang, X., Yang, X., Chen, J., and Chen, Y.: Temporal variations in the hygroscopicity and mixing state of black carbon aerosols in a polluted megacity area, Atmos. Chem. Phys., 18, 15201-15218, doi:10.5194/acp-18-15201-2018, 2018.

Li, L., Li, M., Huang, Z., Gao, W., Nian, H., Fu, Z., Gao, J., Chai, F., and Zhou, Z.: Ambient particle characterization by single particle aerosol mass spectrometry in an urban area of Beijing, Atmos. Environ., 94, 323-331, doi:10.1016/j.atmosenv.2014.03.048, 2014.

Liu, D., Joshi, R., Wang, J., Yu, C., Allan, J. D., Coe, H., Flynn, M. J., Xie, C., Lee, J., Squires, F., Kotthaus, S., Grimmond, S., Ge, X., Sun, Y., and Fu, P.: Contrasting physical properties of black carbon in urban Beijing between winter and summer, Atmos. Chem. Phys., 19, 6749-6769, doi:10.5194/acp-19-6749-2019, 2019.

Lu, S., Tan, Z., Liu, P., Zhao, H., Liu, D., Yu, S., Cheng, P., Win, M. S., Hu, J., Tian, L., Wu, M., Yonemochi, S., and Wang, Q.: Single particle aerosol mass spectrometry of coal combustion particles associated with high lung cancer rates in Xuanwei and Fuyuan, China, Chemosphere, 186, 278-286, doi:10.1016/j.chemosphere.2017.07.161, 2017.

Moffet, R. C., de Foy, B., Molina, L. T., Molina, M. J., and Prather, K. A.: Measurement of ambient aerosols in northern Mexico City by single particle mass spectrometry, Atmos. Chem. Phys., 8, 4499–4516, doi:10.5194/acp-8-4499-2008, 2008.

Pratt, K. A., DeMott, P. J., French, J. R., Wang, Z., Westphal, D. L., Heymsfield, A. J., Twohy, C. H., Prenni, A. J., and Prather, K. A.: In situ detection of biological particles in cloud ice-crystals, Nat. Geosci., 2, 398-401, doi:10.1038/ngeo521, 2009.

Silva, P. J., Liu, D. Y., Noble, C. A., and Prather, K. A.: Size and Chemical Characterization of Individual Particles Resulting from Biomass Burning of Local Southern California Species, Environ. Sci. Technol., 33, 3068-3076, doi:10.1021/es980544p 1999.

Spencer, M. T., Shields, L. G., and Prather, K. A.: Simultaneous Measurement of the Effective Density and Chemical Composition of Ambient Aerosol Particles, Environ. Sci. Technol., 41, 1303-1309, doi:10.1021/es061425+ 2007.

Sun, J., Li, Y., Xu, W., Zhou, W., Du, A., Li, L., Du, X., Huang, F., Li, Z., Zhang, Z., Wang, Z., and Sun, Y.: Single-particle volatility and implications for brown carbon absorption in Beijing, China, Sci. Total Environ., 854, 158874, doi:10.1016/j.scitotenv.2022.158874, 2022a.

Sun, J., Sun, Y., Xie, C., Xu, W., Chen, C., Wang, Z., Li, L., Du, X., Huang, F., Li, Y., Li, Z., Pan, X., Ma, N., Xu, W., Fu, P., and Wang, Z.: The chemical composition and mixing state of BC-containing particles and the implications on light absorption enhancement, Atmos. Chem. Phys., 22, 7619-7630, doi:10.5194/acp-22-7619-2022, 2022b.

Toner, S. M., Sodeman, D. A., and Prather, K. A.: Single particle characterization of ultrafine and accumulation mode particles from heavy duty diesel vehicles using aerosol time-of-flight mass spectrometry, Environ. Sci. Technol., 40, 3912-3921, doi:10.1021/es051455x, 2006.

Toner, S. M., Shields, L. G., Sodeman, D. A., and Prather, K. A.: Using mass spectral source signatures to apportion exhaust particles from gasoline and diesel powered vehicles in a freeway study using UF-ATOFMS, Atmospheric Environment, 42, 568-581, doi:10.1016/j.atmosenv.2007.08.005, 2008.

Wang, H., An, J., Shen, L., Zhu, B., Xia, L., Duan, Q., and Zou, J.: Mixing state of ambient aerosols in Nanjing city by single particle mass spectrometry, Atmos. Environ., 132, 123-132, doi:10.1016/j.atmosenv.2016.02.032, 2016.

Xie, C., He, Y., Lei, L., Zhou, W., Liu, J., Wang, Q., Xu, W., Qiu, Y., Zhao, J., Sun, J., Li, L., Li, M., Zhou, Z., Fu, P., Wang, Z., and Sun, Y.: Contrasting mixing state of black carbon-containing particles in summer and winter in Beijing, Environ. Pollut., 263, 114455, doi:10.1016/j.envpol.2020.114455, 2020.

Zhang, G., Bi, X., Lou, S., Li, L., Wang, H., Wang, X., Zhou, Z., Sheng, G., Fu, J., and Chen, C.: Source and mixing state of iron-containing particles in Shanghai by individual particle analysis, Chemosphere, 95, 9-16, doi:10.1016/j.chemosphere.2013.04.046, 2014.

Zhang, T., Claeys, M., Cachier, H., Dong, S., Wang, W., Maenhaut, W., and Liu, X.: Identification and estimation of the biomass burning contribution to Beijing aerosol using levoglucosan as a molecular marker, Atmos. Environ., 42, 7013-7021, doi:10.1016/j.atmosenv.2008.04.050, 2008.

Zhang, Y., Pei, C., Zhang, J., Cheng, C., Lian, X., Chen, M., Huang, B., Fu, Z., Zhou, Z., and Li, M.: Detection of polycyclic aromatic hydrocarbons using a high performance-single particle aerosol mass spectrometer, J. Environ. Sci., 124, 806-822, doi:10.1016/j.jes.2022.02.003, 2022.

Zhong, Q., Cheng, C., Li, M., Yang, S., Wang, Z., Yun, L., Liu, S., Mao, L., Fu, Z., and Zhou, Z.: Insights into the different mixing states and formation processes of amine-containing single particles in Guangzhou, China, Sci. Total. Environ., 846, 157440, doi:10.1016/j.scitotenv.2022.157440, 2022.